Effects of the computational domain on the secondary flow in turbulent plane Couette flow*

Gai Jie(盖 杰)[a], Xia Zhen-Hua(夏振华)[a)b)†], and Cai Qing-Dong(蔡庆东)[a)‡]

[a)] State Key Laboratory of Turbulence and Complex Systems, Center for Applied Physics and Technology, College of Engineering, Peking University, Beijing 100871, China

[b)] Department of Aeronautics and Astronautics, College of Engineering, Peking University, Beijing 100871, China

(Received 19 January 2015; revised manuscript received 19 April 2015; published online 20 August 2015)

A series of direct numerical simulations of the fully developed plane Couette flow at a Reynolds number of 6000 (based on the relative wall speed and half the channel height h) with different streamwise and spanwise lengths are conducted to investigate the effects of the computational box sizes on the secondary flow (SF). Our focuses are the number of counter-rotating vortex pairs and its relationship to the statistics of the mean flow and the SF in the small and moderate computational box sizes. Our results show that the number of vortex pairs is sensitive to the computational box size, and so are the slope parameter, the rate of the turbulent kinetic energy contributed by the SF, and the ratio of the kinetic energy of the SF to the total kinetic energy. However, the averaged spanwise width of each counter-rotating vortex pair in the plane Couette flow is found, for the first time, within $4(1\pm0.25)h$ despite the domain sizes.

Keywords: plane Couette flow, the secondary flow, large-scale structures, vortex pair

PACS: 47.27.N–, 47.27.ek **DOI:** 10.1088/1674-1056/24/10/104701

1. Introduction

Wall-bounded turbulent flows are of great importance in both theoretical research and engineering applications. As one of the canonical problems, the turbulent plane Couette flow (PCF) (see Fig. 1) has been studied extensively.[1–12] Unlike the pressure-driven plane channel flow, the mean pressure gradient in the PCF is zero, and the flow is driven by the shear generated at the two walls, resulting in a monotonic velocity profile and a constant shear stress distribution at all positions across the channel.

Another distinct difference from the plane channel flow is the large-scale counter-rotating streamwise vortices existing in the PCF core region. These large-scale structures (LSSs) have also been observed in experimental measurements,[13–15] as well as in the numerical simulations.[16–23] Based on a direct numerical simulation (DNS) of a PCF at a Reynolds number $Re_w = U_w h/\nu$ (here, U_w is the velocity difference between the two surfaces, h is half the gap width, and ν is the kinematic viscosity) of 6000 and in a computational box of $4\pi h \times 2h \times 8\pi/3h$, Lee and Kim[16] reported that there are LSSs in the core region, which are extremely long in the flow direction and fill the entire channel. They also found that these LSSs have a spanwise wavelength $\lambda_z/h \simeq 4$. In addition, because the large-scale structures are persistent in space and time, Lee and Kim[16] and Papavassilious[19] approximated the large-scale structures by an SF, which represents the large eddy motion independent of time and streamwise direction. Lee and Kim reported that the SF (or the LSSs) contributes about 30% of the turbulent energy, and Papavassilious,[19] using a computational box of $4\pi h \times 2h \times 2\pi h$, concluded that the SF accounted for up to 40% of the convective transport of streamwise momentum, indicative of the importance of the SF in energetics.

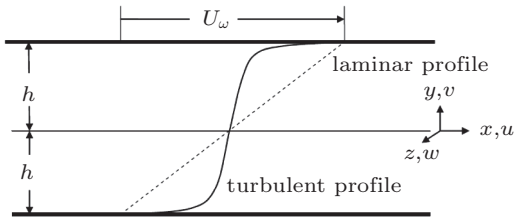


Fig. 1. Schematic diagram of the flow geometry of PCF. The solid line and the dotted line are mean velocity profile in a turbulence flow and a laminar flow, respectively.

Nevertheless, because of the long persistence of the LSSs in the streamwise direction, special attention needs to be paid to the domain sizes when the PCF is studied using the numerical approaches. Bech and Andersson[17] simulated the PCF using three different DNSs at $Re_w = 2600$ with varying computational boxes ($4\pi h \times 2h \times 2\pi h$, $16\pi h \times 2h \times 2\pi h$, and $10\pi h \times 2h \times 4\pi h$) and numerical resolutions. They found that the computational domain size has a great impact on the LSSs and statistics. However, the short sampling time in one of the three DNSs and the varying grid resolution weakened the reliability of the conclusions. Komminaho *et al.*[18] studied the effect of the computational domain on the LSSs in the PCF at

*Project supported by the National Natural Science Foundation of China (Grant Nos. 11221061, 11272013, and 11302006).

†Corresponding author. E-mail: xiazh1006@gmail.com

‡Corresponding author. E-mail: caiqd@pku.edu.cn

© 2015 Chinese Physical Society and IOP Publishing Ltd

$Re_w = 1500$ using DNSs on three different domain sizes, i.e., $8h \times 2h \times 4h$, $10\pi h \times 2h \times 4\pi h$, and $28\pi h \times 2h \times 8\pi h$. The final grid resolutions were kept the same, which were comparable to that in the turbulent channel flow simulation by Kim, Moin and Moser[24] in wall units. Different pairs of the LSSs were observed from their simulations with different domain sizes, and the LSSs from the simulation under the largest box were neither stationary in time nor fixed in position, in sharp contrast to the earlier observations by Lee and Kim[16] with a much smaller box. The statistical quantities for the largest box size, such as the time- and (x,z)-plane-averaged $u_{\rm rms}$ values, were found to converge to the value for an infinite box, indicating that a large enough box size is required to obtain a satisfactory turbulent statistics. Tsukahara *et al.*[20] conducted a series of DNSs of the PCF with various box sizes to investigate the LSSs in the core region. Two Reynolds numbers ($Re_w = 1500$ and 4300) together with four different box sizes were chosen, including $48h \times 2h \times 12h$, $64h \times 2h \times 16h$, $89.6h \times 2h \times 25.6h$, and $128h \times 2h \times 12h$. They concluded that the meandering of the LSSs could be captured with a long box size ($L_x \gtrsim 64h$) in the core region, and the length scale in the spanwise direction should be at least $16h$ to avoid the LSSs being strictly confined by the periodic boundary conditions. Also, they observed that the LSSs, which are made up of counter-rotating streamwise vortex pairs, occupy the whole channel, in agreement with the previous reported results. Although more and more DNSs have been conducted to simulate the PCF nowadays, the influence of the computational domain size upon the LSSs and upon the statistics is not yet completely understood.

To gain more insight into the role which LSSs play in the PCF, it is significant to pay attention to the SF. In the present work, a series of DNSs of the PCF with different computational box lengths have been carried out to examine their effects on the SF. The DNS of the PCF in the large box size is so expensive that it is important and necessary to study the SF behavior and the statistics of the PCF in the small or moderate box size, which may help to predict the turbulent behavior in the large computational domain. Therefore, unlike the previous pioneering studies, the computational domains in the present study are limited to small and moderate sizes, and our focuses are the number of counter-rotating vortex pairs and its relationship to the statistics of the mean flow and the SF. The paper is organized as follows. Details on the numerical procedures are provided in Section 2. Results of the simulation of the PCF are discussed in Section 3, and conclusions are finally provided in Section 4.

2. The numerical method and validation

In the simulations, the bottom wall is fixed, while the upper wall is moved in the streamwise direction at speed U_w (see Fig. 1). The incompressible Navier–Stokes equations are solved using the well-known KMM method,[24] a pseudo-spectral method with Fourier and Chebyshev polynomial expansions in the streamwise and spanwise (x,z) and wall-normal (y) directions, respectively. The equations are integrated in time by using a semi-implicit scheme: a second-order Adams–Bashforth scheme for the nonlinear term and a second-order Crank–Nicolson scheme for the linear term. The nonlinear term is dealiased by using a $3/2$-truncation rule. No-slip condition is used at the walls, and periodic boundary conditions are employed in the horizontal directions.

Table 1. Parameters of the simulations at $Re_w = 6000$. L_x and L_z are the streamwise and spanwise lengths of the numerical box, respectively. $Re_\tau = u_\tau \delta/\nu$ is the Reynolds number based on friction velocity u_τ. N_x, N_y, and N_z are the number of collocation points, and $N_y = 128$ for all cases. Δx^+ and Δz^+ are the spatial resolution. $U_w T/L_x$ is the sampling time.

Case	Re_τ	L_x/h	L_z/h	N_x	N_z	Δx^+	Δz^+	$U_w T/L_x$	Ψ	$R_{k^s/k}$	$R_{k^s/K}$
C22	172.2	2π	2π	64	128	16.9	8.4	79.62	0.136	0.270	0.00685
C24	171.5	2π	4π	64	256	16.8	8.4	79.62	0.125	0.262	0.00621
C41	172.2	4π	$3\pi/2$	128	96	16.9	8.4	59.71	0.118	0.263	0.00667
C42	169.1	4π	2π	128	128	16.6	8.3	59.71	0.203	0.098	0.00212
C43	173.7	4π	3π	128	192	17.0	8.5	59.71	0.090	0.305	0.00809
C44	171.3	4π	4π	128	256	16.8	8.4	59.71	0.148	0.256	0.00635
C82	168.6	8π	2π	256	128	16.5	8.3	45.78	0.207	0.067	0.00145
C84	169.0	8π	4π	256	256	16.6	8.3	31.45	0.197	0.094	0.00209
Lee and Kim	170.0	4π	$8\pi/3$	128	192	16.7	7.4	–	–	0.300	–

In Table 1, we list the parameters of the simulations at $Re_w = 6000$. Eight computational cases with different streamwise lengths L_x and different spanwise widths L_z are simulated with the same resolutions, which are very close to those used by Lee and Kim.[16] The relative friction Reynolds number is $Re_\tau = u_\tau h/\nu \approx 170$, where $u_\tau = \sqrt{\tau_w/\rho}$ is the friction velocity. Non-dimensionalization with wall variables (or inner units) is used appropriately and denoted by a plus superscript, e.g., $y^+ = y u_\tau/\nu$ and $\langle u \rangle^+ = \langle u \rangle / u_\tau$.

Generally, in the research of turbulence, the instantaneous velocity u_i is decomposed into the mean flow $\langle u_i \rangle$, where $\langle \cdot \rangle$ denotes the time- and (x,z)-plane-average scheme, and the fluctuation velocity u_i' (see Eq. (1))

$$u_i(x,y,z,t) = \langle u_i \rangle(y) + u_i'(x,y,z,t). \tag{1}$$

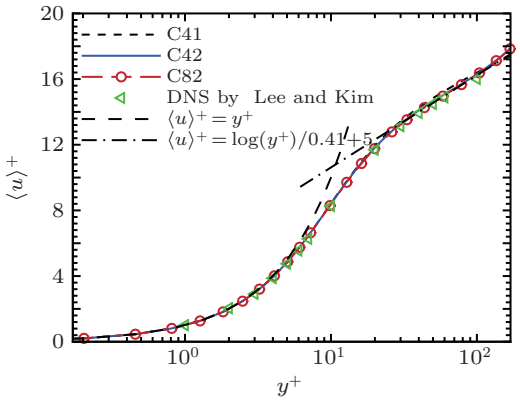


Fig. 2. (color online) Mean streamwise velocity profile normalized by u_τ for case C41 (dashed-line), C42 (solid-line), C82 (long-dashed-line with circles), and by Lee and Kim[16] (◁). The long dashed-line and dash–dotted line denote the law of wall: $\langle u\rangle^+ = y^+$ and $\langle u\rangle^+ = \log(y^+)/\kappa + B$, respectively, where $\kappa = 0.41$ and $B = 5.0$.

We display the normalized mean velocity profiles in wall scales from the cases C41, C42, and C82 in Fig. 2, as well as that from Lee and Kim.[16] It is apparent that the velocity profiles from the three cases agree very well with that from Lee and Kim, indicating that the present code and simulations are reliable.

3. Results and discussion

In the present paper, for investigating the characteristics associated with the SF (or the large-eddy motions), the instantaneous velocity u_i is decomposed by a triple-decomposition approach[16,19]

$$\begin{aligned} u_i(x,y,z,t) &= \langle u_i\rangle(y) + u_i^{\mathrm{s}}(y,z) + u_i''(x,y,z,t), \\ &= \langle u_i\rangle(y) + u_i'(x,y,z,t). \end{aligned} \tag{2}$$

Here, u_i^{s} is the velocity field corresponding to the SF, which is obtained by averaging the velocity over time and the x direction and subtracting its mean value $\langle u_i\rangle$. For clarity, we call $u_i' = u_i - \langle u_i\rangle = u_i^{\mathrm{s}} + u_i''$ the fluctuation velocity and u_i'' the velocity of the residual field,[16] respectively.

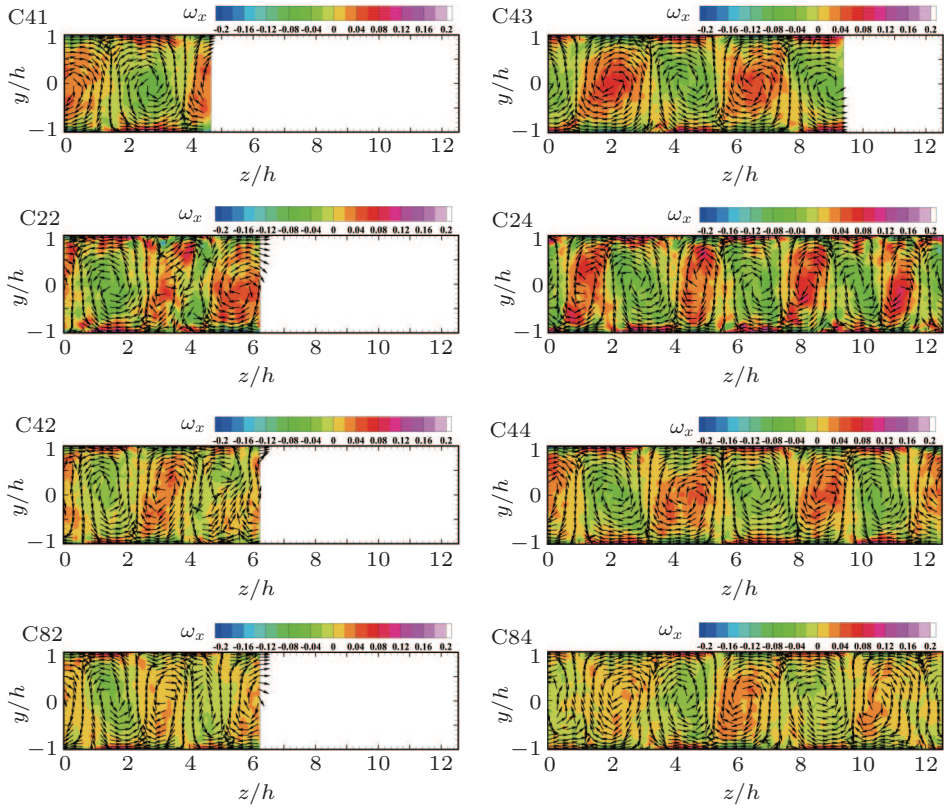


Fig. 3. (color online) Velocity vectors of the SF, $(v^{\mathrm{s}}, w^{\mathrm{s}})$, and streamwise vorticity, ω_x, in the yz-plane for eight computational cases (as listed in Table 1).

In Fig. 3, the SF for eight cases are shown in the yz-plane, and the counter-rotating vortex pairs can be counted clearly. As Lee and Kim reported, the large-scale eddies are indeed so large that they fill the whole channel. By getting results from Fig. 3, the number of vortex pairs N_{vp} and a vortex wavelength (or mean spanwise scale of vortex pairs) $\lambda_z = L_z/N_{\mathrm{vp}}$ for eight cases are summarized in Table 2. In addition, it indicates that the number of the vortex pairs is sensitive to the computational box size, and it may highly influence the statistics of turbulence. On the other hand, let us consider cases C22, C42, and C82 which have the same spanwise width $L_z = 2\pi h$. For case C82, the velocity vectors of the secondary flow are very neat. However, for cases C22 and C42, the secondary flows are not smooth, even though the velocity fields are averaged over a

double period of the sampling time (as listed in Table 1). We prefer to attribute this non-smooth behavior of the secondary flows to the unfavorable domain size which may prevent the formation of persistent vortices.[25]

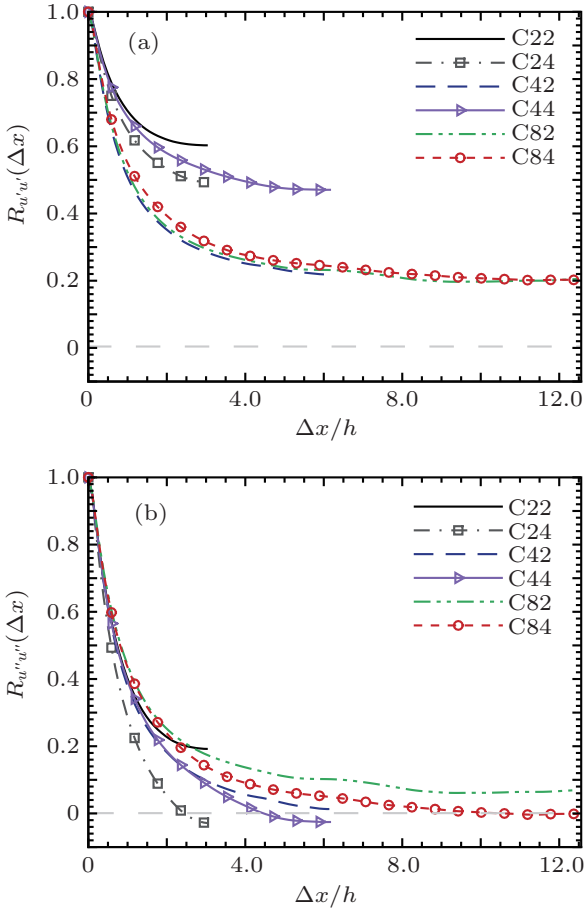


Fig. 4. (color online) The two-point streamwise correlation (a) for the streamwise fluctuation velocity $R_{u'u'}$, (b) for the streamwise velocity of residual field $R_{u''u''}$, at $y = 0$ for different box sizes: cases C22, C24, C42, C82, and C84.

Generally, the influence of box size on the LSSs can be observed by the two-point streamwise correlation for the streamwise fluctuation velocity $R_{u'u'}(\Delta x)$. Besides, in the present paper, the two-point streamwise correlation for the streamwise velocity of residual field $R_{u''u''}(\Delta x)$ is applied to study the effect of the SF. We plot $R_{u'u'}(\Delta x)$ and $R_{u''u''}(\Delta x)$, at the centerline, in Fig. 4(a) and Fig. 4(b), respectively, for six cases (case C22, C24, C42, C44, C82, and C84).

$$R_{u'u'}(\Delta x_i) = \frac{\langle u'(x_i)u'(x_i+\Delta x_i)\rangle}{\langle u'(x_i)u'(x_i)\rangle}, \tag{3}$$

$$R_{u''u''}(\Delta x_i) = \frac{\langle u''(x_i)u''(x_i+\Delta x_i)\rangle}{\langle u''(x_i)u''(x_i)\rangle}. \tag{4}$$

As shown in Fig. 4(a), $R_{u'u'}(\Delta x)$ for six cases all remain positive at the mid box length because of the small box size. In Fig. 4(b), $R_{u''u''}(\Delta x)$ for six cases are all obviously smaller than $R_{u'u'}(\Delta x)$, and, specially, $R_{u''u''}(\Delta x)$ for cases C24, C44, and C84 reach negative at the mid box length. It indicates that there is a strong secondary flow in the PCF. In addition, $R_{u'u'}(\Delta x)$ for case C84 is smaller than $R_{u'u'}(\Delta x)$ for case C44 which has the same spanwise computational width as case C84, while $R_{u'u'}(\Delta x)$ for cases C42 and C82 are almost equal. It means that, on the condition of the wider computational width L_z, we need to compute with the longer computational length L_x to capture the one period of the streamwise structure. What is more, $R_{u'u'}(\Delta x)$ for cases C42, C82, and C84 almost collapse, and $R_{u'u'}(\Delta x)$ for cases C82 and C84 are constant when Δx is larger than $10h$. Therefore, we predict that, for the computational widths of $2\pi h$ and $4\pi h$, the two-point streamwise correlation $R_{u'u'}(\Delta x)$ cannot reach the negative at the mid box length, even though the computational length is much longer than $8\pi h$. It indicates that the box width L_z must be long enough, at least larger than $4\pi h$, to ensure that we can capture the one period of the streamwise structure.

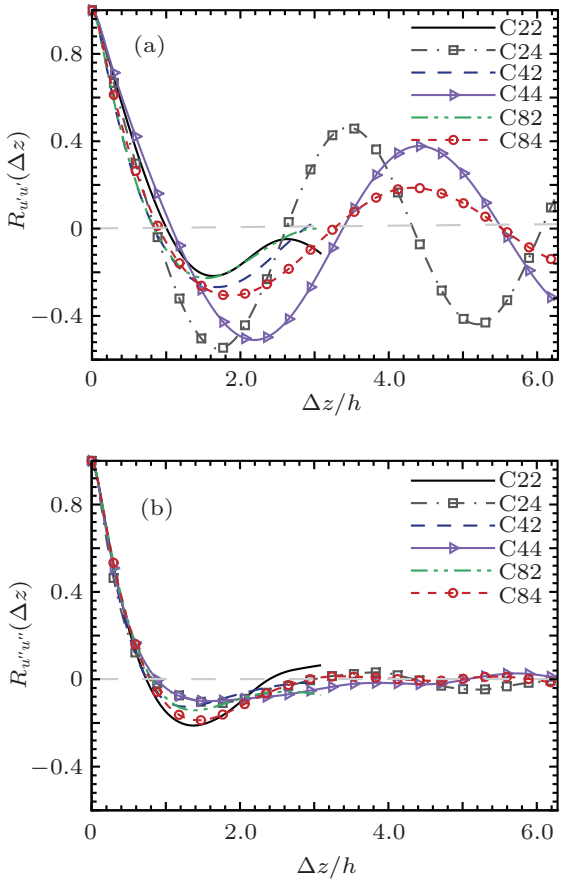


Fig. 5. (color online) The two-point spanwise correlation (a) for the streamwise fluctuation velocity $R_{u'u'}$, (b) for the streamwise velocity of residual field $R_{u''u''}$, at $y = 0$ for different box sizes: cases C22, C24, C42, C82, and C84.

The two-point spanwise correlations $R_{u'u'}(\Delta z)$ and $R_{u''u''}(\Delta z)$, at the center of the channel, are given in Fig. 5(a) and Fig. 5(b), respectively. In Fig. 5(a), the strongest minimum of $R_{u'u'}(\Delta z)$ for cases C24 and C44 are smaller than that for case C84, which verifies that a long box length L_x is necessary to weaken the effect of the periodic boundary condition,

and it leads to a reduction of the spanwise correlation for the LSSs. The magnitude of $R_{u''u''}(\Delta z)$ is much smaller than that of $R_{u'u'}(\Delta z)$, as shown in Fig. 5(b), by which we confirm there is a strong secondary flow in the PCF.

The normalized velocity gradient at the centerline (CL), also called the slope parameter, defined as

$$\Psi = \frac{2h}{|\langle u\rangle_{y=h} - \langle u\rangle_{y=-h}|}\left.\frac{\mathrm{d}\langle u\rangle}{\mathrm{d}y}\right|_{\mathrm{CL}} = \frac{2h}{U_w}\left.\frac{\mathrm{d}\langle u\rangle}{\mathrm{d}y}\right|_{\mathrm{CL}}, \tag{5}$$

is a characteristic parameter of the PCF, which is a measurement of the mean velocity field to a certain degree. However, its dependence on the Reynolds number is still an open question in the PCF.[22] The value of Ψ at infinite Reynolds number was suggested to be 0.25 by Busse,[26] and 0 by Lund and Bush,[27] respectively. On the other hand, several experiments and DNSs at low Reynolds numbers or with very small boxes suggested the values are close to the range 0.18–0.2.[13,18,20] Avsarkisov *et al.*[22] found a clear decrease trend of this value, with $\Psi = 0.18$, 0.16, 0.14, and 0.1 for $Re_w = 4500$, 6300, 9000, and 22500. In the present simulations, we simulated one Reynolds number, and Ψ should be a single value in a large enough computational domain. However, because of the strong and unsteady behavior of the SF, at the same Reynolds number, the values of Ψ are scattered within a range of 0.090–0.207 in the small computational domains, as listed in Table 1.

Under the triple-decomposition, the total kinetic energy $K \equiv \langle u_i u_i\rangle/2$ (the repeated subscripts imply summation) can be decomposed into three parts, similarly:

$$K = \frac{1}{2}\langle u_i\rangle\langle u_i\rangle + \frac{1}{2}\langle u_i^{\mathrm{s}}u_i^{\mathrm{s}}\rangle + \frac{1}{2}\langle u_i''u_i''\rangle, \tag{6}$$

i.e., the kinetic energy of the mean flow $\langle u_i\rangle\langle u_i\rangle/2$, the kinetic energy of the SF $k^{\mathrm{s}} \equiv \langle u_i^{\mathrm{s}}u_i^{\mathrm{s}}\rangle/2$, and the kinetic energy of the residual field $k'' \equiv \langle u_i''u_i''\rangle/2$. Here, the turbulent kinetic energy is

$$k \equiv \frac{1}{2}\langle u_i'u_i'\rangle = k^{\mathrm{s}} + k''. \tag{7}$$

In order to study the importance of the SF in energetic, we further define two parameters:

$$R_{k^{\mathrm{s}}/k} = \int_{-h}^{h} k^{\mathrm{s}}(y)\,\mathrm{d}y \Big/ \int_{-h}^{h} k(y)\,\mathrm{d}y\,, \tag{8}$$

$$R_{k^{\mathrm{s}}/K} = \int_{-h}^{h} k^{\mathrm{s}}(y)\,\mathrm{d}y \Big/ \int_{-h}^{h} K(y)\,\mathrm{d}y\,, \tag{9}$$

i.e., the rate of the turbulent kinetic energy contributed by the SF and the ratio of the kinetic energy of the SF to the total kinetic energy. The values of $R_{k^{\mathrm{s}}/k}$ and $R_{k^{\mathrm{s}}/K}$ from our simulations are listed in the last two columns of Table 1. Similar to the slope parameter, these two ratios are scattered, within the range of 0.067–0.305, and 0.00145–0.00685, respectively. Lee and Kim[16] reported that $R_{k^{\mathrm{s}}/k} \sim 30\%$, and the case of C43, which employs a similar computational box, has the closest value of $R_{k^{\mathrm{s}}/k} \simeq 30.5\%$. Through the statistics of $R_{k^{\mathrm{s}}/k}$, it indicates that the rate of the turbulent kinetic energy contributed by the SF is much lower than 30% in the large computational domain.

Since the total input of the PCF is the momentum from the upper moving wall, which is a constant, the total kinetic energy should be the same at the fully developed state. In particular, in the cases of C22, C42, and C82, the values of $R_{k^{\mathrm{s}}/K}$ decrease as L_x increases, and this could be explained by the fact that the self-amplification mechanism becomes weaker as L_x increases, as pointed out by Komminaho[18] and Andersson,[9] which results in weakened large-eddy motions. However, the above-mentioned dependence on L_x is not exactly true for the cases C24, C44, and C84, but it is true for the cases C44 and C84. The reason can be related to the different numbers of the counter-rotating vortex pairs in the cases C24, C44, and C84 (see Table 2). Different spanwise and streamwise lengths will obtain different numbers of the counter-rotating vortex pairs in the simulation of PCF, resulting in different intensities of the SF. This is exactly the reason for the unclear dependence of the values of $R_{k^{\mathrm{s}}/K}$ on L_z.

Clearly, the statistical quantities discussed above, i.e., the slope parameter, $R_{k^{\mathrm{s}}/K}$ and $R_{k^{\mathrm{s}}/k}$, are not convergent in the present simulations and are highly influenced by the computational domain size, which may be affected by the SF primarily. It is expected, at least intuitively, that more pairs of counter-rotating vortices (a manifestation of the SF) could be obtained if the spanwise length of the computational box was wider. Earlier simulations by Kimminaho *et al.*[18] observed one pair of counter-rotating vortices when the domain was $8h \times 2h \times 4h$, and six pairs when the domain was $28\pi h \times 2h \times 8\pi h$. In the present simulations, we also get different pairs of counter-rotating vortices with different computational boxes. In Table 2, we list the number of vortex pairs N_{vp} and the average width λ_z of vortex pairs from all the present simulations, as well as the data from previous simulations, including those from Lee and Kim,[16] Komminaho *et al.*,[18] Avsarkisov *et al.*,[22] Bernardini *et al.*,[12] and Narasimhamurthy *et al.*[28]

In Fig. 6(a), we plot the number of vortex pairs N_{vp} from all the data, listed in Table 2. As discussed above, more pairs of counter-rotating vortices are obtained with a wider spanwise width of the computational domain, as expected, except case C24, where four pairs of vortices are observed with $L_x = 2\pi h$ and $L_z = 4\pi h$. This means that the streamwise length may also influence the SF to some extent.

Table 2. The number of vortex pairs N_{vp} and the averaged width $\lambda_z = L_z/N_{vp}$ of each pair for all the cases. L-K is the result from Lee and Kim,[16] K-L-J are the results from Komminaho *et al.*,[18] A-H-O-G is the result from Avsarkisov *et al.*,[22] B-P-O is the result from Bernardini *et al.*,[12] and N-A-P is the result from Narasimhamurthy *et al.*[28] All quantities are normalized by h.

Case	C41	C22	C42	C82	C43	C24	C44	C84
L_x/h	4π	2π	4π	8π	4π	2π	4π	8π
L_z/h	$3\pi/2$	2π	2π	2π	3π	4π	4π	4π
N_{vp}	1	2	2	2	2	4	3	3
λ_z/h	1.5π	π	π	π	1.5π	π	1.33π	1.33π
Case	L-K	K-L-J	K-L-J	A-H-O-G	B-P-O	N-A-P		
L_x/h	4π	8	28π	20π	12π	16π		
L_z/h	$8\pi/3$	4	8π	6π	4π	5.35π		
N_{vp}	2	1	6	4	3	4		
λ_z/h	1.33π	4	1.33π	1.5π	1.33π	1.34π		

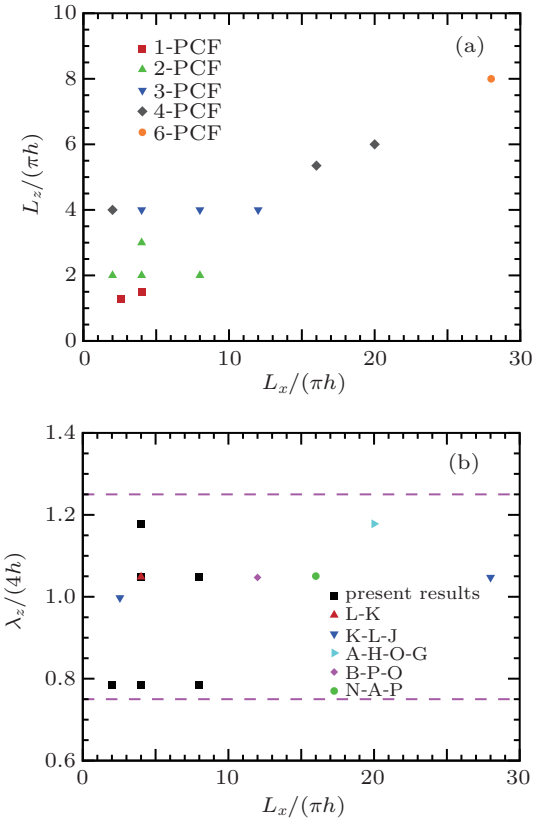


Fig. 6. (color online) (a) Phase diagram of the number of counter-rotating vortex pairs with different streamwise length L_x/π and the spanwise width L_z/π. The numbers are shown in front of the mapping names. (b) Scatter diagram of the normalized averaged width of each vortex pair $\lambda_z/4$ as a function of the streamwise length L_x/π. The mapping names denote the data resources.

The averaged spanwise width of each counter-rotating pair $\lambda_z = L_z/N_{vp}$ varies within a certain range $4(1\pm0.25)h$, despite the computational box size, as shown in Fig. 6(b), where the normalized averaged width of each vortex pair $\lambda_z/(4h)$ is shown as a function of the streamwise length $L_x/h/\pi$. In the PCF, the large-scale eddies fill the entire channel, and the height of the counter-rotating vortex pair is $2h$. If the averaged width of each large-eddy was $2h$, then the large-eddy had equal width and height, approximating to a circle shape. The averaged spanwise width of each pair is $4(1\pm0.25)h$, i.e., the averaged spanwise width of each vortex is $2(1\pm0.25)h$, indicating that the large-eddies are inclined to the circle shape in all the cases. In fact, in free-shear flow problems without solid boundaries, the large-eddy or vortex tends to a circle shape due to the centrifugal force. Because of the existence of the wall (non-slip boundary conditions), the large-eddies in the PCF show a little variance.

4. Conclusions

In the present work, a series of DNSs of the fully developed PCF at Reynolds number $Re_w = 6000$ with different streamwise and spanwise lengths are conducted to investigate the effect of the computational box sizes on the SF. Our focuses are the number of counter-rotating vortex pairs and its relationship to the statistics of the mean flow and the SF under small and moderate computational box sizes. The results lead to the following conclusions.

(i) The number of the counter-rotating vortex pairs is sensitive to the computational box sizes, and so are the slope parameter, the rate of the turbulent kinetic energy contributed by the SF, and the ratio of the kinetic energy of the secondary to the total kinetic energy. It is exactly indicated that no convergent conclusion could be made for the PCF using the different small box sizes, which is caused by the strong and unsteady behavior of the SF.

(ii) Based on the data from the present simulations and the previous available DNSs, the averaged spanwise width of each counter-rotating vortex pair in the PCF is found, for the first time, within $4(1\pm0.25)h$ despite the domain sizes.

Clearly, the different computational box sizes result in different large-scale vortex structures and different statistical quantities of the PCF. In the future, we will study the underlying reason for relationship between the SF and the computational box sizes.

References

[1] Aydin M and Leuthusser H J 1979 *Rev. Sci. Instrum.* **50** 1362
[2] El Telbany M M M and Reynolds A J 1982 *J. Fluids Eng.* **104** 367

[3] Andersson H I, Bech K H and Kristoffersen R1992 *Proc. Roy. Soc. Lond. Ser. A: Math. Phys. Sci.* **438** 477

[4] Kristoffersen R, Bech K H and Andersson H I1993 *Appl. Sci. Res.* **51** 337

[5] Tillmark N and Alfredsson P H 1993 *Appl. Sci. Res.* **51** 237

[6] Bech K H, Tillmark N, Alfredsson P H and Andersson H I 1995 *J. Fluid Mech.* **286** 291

[7] Hamilton J M, Kim J and Walffe F 1995 *J. Fluid Mech.* **287** 317

[8] Bech K H and Andersson H I 1996 *Fluid Dyn. Res.* **18** 65

[9] Andersson H I, Lygren M and Kristoffersen R 1998 *Proceedings of the* 16*th International Conference on Numerical Methods in Fluid Dynamics*, July 6–7, 1998, Arcachon, France, pp. 117–122

[10] Umeki M and Kitoh O 2008 *IUTAM Symposium on Computational Physics and New Perspectives in Turbulence*, September 11–14, 2006, Nagoya, Japan, pp. 215–220

[11] Tsukahara T, Kawaguchi Y and Kawamura H 2009 *Advances in Turbulence XII*, September 7–10, 2009, Marburg, Germany, pp. 71–74

[12] Bernardini M, Pirozzoli S and Orlandi P 2013 *Int. J. Multiphase Flow* **51** 55

[13] Tillmark N 1995 "Experiments on transition and turbulence in plane Couette flow", Ph. D. Dissertation (Royal Institute of Technology)

[14] Kitoh O, Nakabyashi K and Nishimura F 2005 *J. Fluid Mech.* **539** 199

[15] Kitoh O and Umeki M 2008 *Phys. Fluids* **20** 025107

[16] Lee M J and Kim J 8*th Symposium on Turbulent Shear Flows*, 1991, Munich, Germany, pp. 5-3-1–5-3-6

[17] Bech K H and Andersson H I 1994 *Direct and Large-Eddy Simulation I* pp. 13–24

[18] Komminaho J, Lundbladh A and Johansson A V 1996 *J. Fluid Mech.* **320** 259

[19] Papavassiliou D V and Hanratty T J 1997 *Int. J. Heat Fluid Flow* **18** 55

[20] Tsukahara T, Kawamura H and Shingai K 2006 *J. Turbulence* **7** 1

[21] Holstad A, Johansson P S, Andersson H I and Pettersen B 2006 *Direct and Large-Eddy Simulation VI* **10** pp. 763–770

[22] Avsarkisov V, Hoyas S, Oberlack M and García-Galache J P 2014 *J. Fluid Mech.* **751** R1

[23] Pirozzoli S, Bernardini M and Orlandi P 2014 *J. Fluid Mech.* **758** 327

[24] Kim J, Moin P and Moser R 1987 *J. Fluid Mech.* **177** 133

[25] Kristoffersen R and Andersson H I 1993 *J. Fluid Mech.* **256** 163

[26] Busse F H 1970 *J. Fluid Mech.* **41** 219

[27] Lund K O and Bush W B 1980 *J. Fluid Mech.* **96** 81

[28] Narasimhamurthy V D, Andersson H I and Pettersen B 2011 *J. Phys.: Conf. Ser.* **318** 022017

[29] Zhao H 2003 "A direct numerical simulation of channel turbulence and its open-loop control by traveling wavy wall", MS Thesis (Beijing: Peking University) (in Chinese)